Hybrid Rotation Averaging: A Fast and Robust Rotation Averaging Approach

Yu Chen Peking University

Ji Zhao TuSimple

Laurent Kneip ShanghaiTech University

hackerdreamer34@gmail.com

zhaoji84@gmail.com

lkneip@shanghaitech.edu.cn

Abstract

We address rotation averaging (RA) and its application to real-world 3D reconstruction. Local optimisation based approaches are the defacto choice, though they only guarantee a local optimum. Global optimisers ensure global optimality in low noise conditions, but they are inefficient and may easily deviate under the influence of outliers or elevated noise levels. We push the envelope of rotation averaging by leveraging the advantages of global RA method and local RA method. Combined with a fast view graph filtering as preprocessing, the proposed hybrid approach is robust to outliers. We apply the proposed hybrid rotation averaging approach to incremental Structure from Motion (SfM) by adding the resulting global rotations as regularisers to bundle adjustment. Overall, we demonstrate high practicality of the proposed method as bad camera poses are effectively corrected and drift is reduced.

1. Introduction

Rotation averaging is a problem that consists of estimating absolute camera orientations that agree as well as possible with a set of pairwise relative orientations. Errors expressing disagreements between estimated absolute orientations and the measured relative orientations are hereby distributed over each pairwise constraint. Rotation averaging is essential in global or hierarchical Structure from Motion (SfM) [29, 15, 36, 49, 50], as well as Simultaneous Localization and Mapping (SLAM) [8] where it can accelerate camera pose estimation and reduce drift accumulation.

In global SfM, we typically start by constructing a view graph \mathcal{G} that encodes all connections between pairs of views i and j by an edge (i,j), each one including the relative motion between image i and image j. Rotation averaging then gives us the absolute orientation of each view, and it is typically followed by a translation averaging step [26, 31, 22, 51] to also obtain absolute positions. Triangulation of 3D points and joint optimisation over all parameters (i.e.

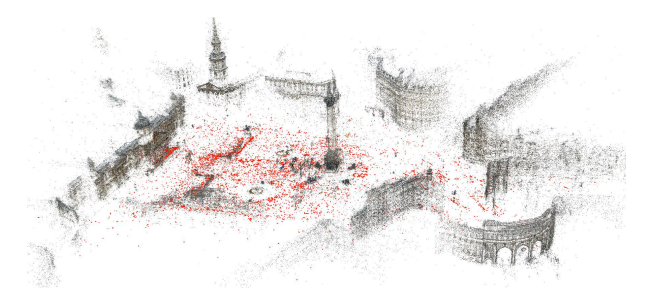


Figure 1. Reconstructions generated from the Trafalgar dataset [45], where 7085 out of 15685 images have been registered.

bundle adjustment [39]) completes the reconstruction. In SLAM, rotation averaging has been used in the back-end pose graph optimisation [33, 8] to flexibly encounter large drift accumulations or—more generally—replace the time-consuming bundle adjustment step.

Rotation averaging was first proposed using the quaternion representation [23]. Later solutions can be categorised into approaches based on either local and global optimisation. Local optimisation approaches such as the one presented by Chatterjee and Govindu [9] are well studied and practical. However, these methods only return the nearest local minimum. To overcome this limitation, the community has also proposed global optimisation approaches [40, 33, 19, 18, 16]. Though the retrieval of global optima can be guaranteed, they have large computational cost and high sensitivity against outliers, and thus are impractical when applied to large-scale SfM problems.

In this paper, we focus on improving the efficiency and robustness of rotation averaging method, and push its application to challenging scenes. We make a combination of global solver and local solver to solve rotation averaging, with global optimality is guaranteed and outliers insensitive. Rotation averaging based on chordal distances can be reformulated as a semi-definite program (SDP) with a low-rank constraint. Taking advantage of low-rank factorisation of original SDP, we can apply the Riemannian-Staircase-based [4] methods, with global optimum guaranteed. In

principle, any global solvers [33, 37, 17] can be used in our hybrid framework, we adopt the block coordinate minimisation method [37] to better leverage the view graph sparsity. By preprocessing the graph with fast view graph filtering, graph sparsity can be further exploited to accelerate the optimisation.

Previous works mainly apply rotation averaging to global SfM. Though global SfM is efficient, translation averaging is often complicated by the unknown scale of relative translations and the difficulty of identifying outliers. In this work, we embed the proposed approach into an incremental SfM pipeline. The strategy is inspired by the work of Cui et al. [13], who propose a hybrid SfM scheme where camera rotations are estimated globally, and camera centers are estimated incrementally by a perspective-2-point (P2P) method. Though the approach is efficient, some globally estimated rotations are not correct preventing camera centers from proper registration and scene reconstructions from completeness. Inspired by Cui's approach [13], we apply rotation averaging in a traditional incremental SfM pipeline, however use the perspective-3-point (P3P) to register camera rotations and centers.

We further propose a novel cost function to optimise camera poses and landmarks that alleviates drift accumulation, in which camera rotations obtained from rotation averaging are used as regularisers. The resulting SfM approach, named RA-SfM (Rotation Averaged Structure from Motion), shows high practicality and at least comparable accuracy, which is demonstrated at the hand of extensive experiments on large-scale real-world datasets.

In summary, the main contributions of our work are:

- We propose a hybrid rotation averaging scheme, which combines the global optimiser with fast view graph filtering and the local optimiser, that is able to robustly handle outliers.
- We refine the traditional incremental bundle adjustment cost function by adding the obtained global rotations as a regularisation term, which significantly alleviates drift accumulation in incremental SfM.

The practicality and superiority of the proposed scheme is demonstrated by extensive experiments on large-scale real-world datasets.

2. Related Work

Motion averaging [23, 24] is widely used in global SfM pipelines [29, 15, 36, 49, 50] as an answer to the drift problem occurring in incremental SfM [3, 46, 34, 14]. The first solution to rotation averaging goes back to Govindu [23], who uses the quaternion representation and solves the problem by linear least-squares fitting. More reliable results were later on gained by optimising over a Lie alge-

bra [24]. In practice, the problem is complicated by the existence of outliers. To enhance the robustness of rotation averaging, absolute rotations may first be initialised under the L_1 -norm, and then refined by Iteratively Reweighted Least Squares (IRLS) [9, 10]. Despite great progress, all aforementioned approaches can only guarantee a locally optimal solution. Another local approach was proposed by Crandall *et al.* [11, 12], who couple the cost function with regularisation terms to enhance robustness. However, the method is computationally demanding as it relies on discrete belief propagation over a Markov random field.

Fredriksson and Olsson [21] exploit Lagrangian duality to become the first to find a globally optimal solution to the rotation averaging problem. In a similar approach, Eriksson *et al.* [18] perform the optimisation directly on the rotation matrix by minimising chordal distances. By removing the determinant constraint on the rotation from the original SDP, they elegantly prove that there is no duality gap between the primal problem and its dual when residual errors are bounded below an angular residual threshold.

Rotation averaging can be converted into an SDP optimisation problem [6]. Wang and Singer [41] solve it by the Alternating Direction Method of Multipliers (ADMM) [5, 44]. Eriksson et al. [18] use a row-by-row block coordinate descent method (BCM) [43]. However, due to the slow convergence of ADMM and the repetitive fill-in procedures of BCM, neither approach proves to be practical when applied to large-scale datasets. A seminal work on the solution of SDP problems is presented by Burer and Monteiro [7], where the positive semi-definite variable is replaced by an appropriate factorisation, and the minimal rank variable is chosen to enhance computational speed. The Burer-Monteiro factorisation later inspired Boumal [4], who proposes a general optimisation technique named the Riemannian staircase algorithm, where the rank variable is augmented until the KKT condition is met, thus guaranteeing global optimality. Rosen et al. [33] address the SDP problem of pose graph optimisation in the Special Euclidean space (SE(n)). When translation variables are decoupled from rotations, they first find the second-order critical point by the second-order Riemannian trust-region method, and then adopt the low-rank optimisation framework of [4] to guarantee global optimality [33]. Inspired by Wang's work et al. [42], which solves the low-rank SDP problem by block coordinate descent method, Tian et al. [37] extends this work to Steifel manifold, and further applied a Riemannian BCM method to pose graph optimisation in distributed settings [38]. Building on SE-Sync [33], Dellaert et al. [16] propose Shonan rotation averaging, a method in which the rotation matrix is vectorized, thus permitting the use of existing gradient-based optimisation methods (e.g. Gauss-Newton or Levenberg-Marquardt) on the manifold of rotation matrices. However, both SE-Sync and Shonan rotation averaging need to evaluate and maintain the Jacobian matrix, which slows down both approaches.

3. Notations and Preliminaries

Let $\mathcal{G}=\{V,E\}$ be an undirected graph, where V represents the collection of nodes and E the set of edges. Let m=|E| be the number of edges and n=|V| be the number of nodes. Let $\operatorname{tr}(\cdot)$ denote the trace of a square matrix. Given two matrices $A\in\mathbb{R}^{m\times n}$ and $B\in\mathbb{R}^{m\times n}$, let $\langle A,B\rangle=\sum_i\sum_jA_{ij}B_{ij}$. We therefore have $\operatorname{tr}(A^TB)=\langle A,B\rangle$. Let $\operatorname{blockdiag}(A)$ represent the block diagonal matrix of A, and $\operatorname{symblockdiag}(A)=\frac{1}{2}\operatorname{blockdiag}(A+A^T)$.

The set of rotations in 3D forms the Special Orthogonal Group SO(3), i.e.,

$$SO(3) = \{ R \in \mathbb{R}^{3 \times 3} | R^T R = I, \det(R) = 1 \}.$$
 (1)

Since SO(3) is a Lie group, there exists an exponential mapping between a rotation R and its Lie algebra $\mathfrak{so}(3)$ representation \boldsymbol{w} [28]:

$$R = \exp([\boldsymbol{w}]_{\times}). \tag{2}$$

The absolute rotations are grouped in $\mathcal{R} = \{R_1, R_2, \cdots, R_n\}$, where $R_i \in SO(3)$, $i \in [n]$. Relative rotations are represented by $\mathcal{R}_{rel} = \{R_{ij}\}$, where $R_{ij} \in SO(3)$, $i, j \in [n]$, i < j is the rotation from R_i to R_j . The chordal distance between two rotations is measured by [25]

$$d_{\text{chord}}(R_1, R_2) = \|R_1 - R_2\|_{E}, \tag{3}$$

where $\|\cdot\|_F$ represents the Frobenius norm of a matrix.

4. Hybrid Rotation Averaging

Globally optimal rotation averaging is sensitive to outliers, thus requiring an additional step to clean the view graph. In this section, we first present an efficient preprocessing step to filter outliers in the view graph. We then apply a block coordinate descent (BCD) method [37] to optimise the low-rank formulation of rotation averaging. Its global optimality can be guaranteed theoretically. Finally, we apply a local optimisation step to further refine the result in the case of scenes that have many erroneous edges.

4.1. Fast View Graph Filtering

The view graph plays an important role in our SfM pipeline. We clean the view graph for two main reasons: (1) Solutions of global rotation averaging algorithms can be biased by outliers. In addition, global optimality is only guaranteed when the residuals for each edge are bounded below a certain threshold [18]. (2) Some view pairs are redundant and even have negative impact on the quality of SfM results. Zach *et al.* [47] proposed a view graph filtering (VGF) technique to obtain a high quality initial view

graph, where loop constraints of rotation triplets are utilised to detect outliers. Specifically, edge (i,j) is an outlier if its angular error satisfies

$$d(R_{ij}R_{jk}R_{ki}, I) > \epsilon. \tag{4}$$

Despite its effectiveness, [47] needs to validate all triplets, which is impractical for large-scale datasets. However, [35] suggests that it is not necessary to check all triplets to distinguish inliers from outliers, and that an increased number of valid 2D-2D image correspondences usually suggests more reliable two-view geometries. We propose an efficient view graph filtering method that relies on this observation. In the following, we denote a group of 3 nodes as a *triplet*, and a triplet with two valid edges and one unverified edge as a *weak triplet*.

Given an initial view graph \mathcal{G} , we start by constructing a maximum spanning tree (MST), where the weight of an edge is the number of valid 2D-2D correspondences. The relative rotations from this MST are all treated as valid. We then check the triplets along with the MST. That is, all adjacent edges that share a common node in the MST are used to build triplets. Next, we generate many weak triplets. Now supposing that edges (i, j) and (j, k) are valid and edge (i, k) exists, we use criterion (4) to verify the validity of edge (i, k). An iteration is completed once all such weak triplets have been verified. After the first iteration, new weak triplets are generated based on which we can perform another iteration. We empirically found that 3 iterations are sufficient for successful rotation averaging.

4.2. Global Rotation Averaging Review

In this section, we first review a globally optimal guaranteed rotation averaging method [37], then the sparsity pattern of the view graph is further exploited to accelerate the algorithm.

Given a set of relative rotations $\{R_{ij}\}$, where $i, j \in [n]$, the aim of rotation averaging is to obtain the absolute rotations $\{R_i\}$ that satisfy the constraints

$$R_{ij} = R_j R_i^{-1} = R_j R_i^T (5)$$

between absolute and relative rotations. Usually there are more edges than nodes in an undirected graph, so there are more constraints than unknowns. Rotation averaging can be formulated as

$$\min_{R_1, \dots, R_n} \sum_{(i,j) \in E} d^p(R_{ij}, R_j R_i^T), \tag{6}$$

where $d^p(\cdot)$ represents a distance measure under a p-norm. While there are a lot of local methods [23, 24, 9, 10] giving a least-squares solution to problem (6), here we exploit a global optimisation approach that can obtain the global optimum.

Chordal distances is popular as the distance measure in (6). Each residual along an edge of \mathcal{G} will hence read

$$||R_{j} - R_{ij}R_{i}||_{F}^{2}$$

$$= ||R_{j}||_{F}^{2} - 2\operatorname{tr}(R_{j}^{T}R_{ij}R_{i}) + ||R_{i}||_{F}^{2}$$

$$= 6 - 2\operatorname{tr}(R_{i}^{T}R_{ij}R_{i}).$$
(7)

The set of absolute rotations can be represented by

$$R = [R_1 R_2 \cdots R_n], \tag{8}$$

and the graph $\mathcal G$ can be represented by

$$G = \begin{bmatrix} 0 & a_{12}R_{12} & \cdots & a_{1n}R_{1n} \\ a_{21}R_{21} & 0 & \cdots & a_{2n}R_{2n} \\ \vdots & \vdots & \ddots & \vdots \\ a_{n1}R_{n1} & a_{n2}R_{n2} & \cdots & 0 \end{bmatrix}, \quad (9)$$

where $a_{ij}=1$ if the edge between views i and j exists, and $a_{ij}=0$ otherwise. By combining Eqs. (7), (8) and (9), problem (6) can be rewritten as

$$\min_{R} (6 - \operatorname{tr}(R^{T}GR)) \Leftrightarrow \min_{R} - \operatorname{tr}(R^{T}GR).$$
 (10)

The primal problem of rotation averaging is finally given by

$$\min_{R} -\operatorname{tr}(R^T G R) \quad \text{s.t.} \quad R \in SO(3)^n.$$
 (11)

Eriksson *et al.* [18] solve the dual problem with determinant constraint relaxation

$$\min_{X} - \operatorname{tr}(GX)$$
s.t. $X_{ii} = I_3, \ i = 1, \cdots, n, \quad X \succeq 0,$ (12)

where X is partitioned as

$$X = \begin{bmatrix} X_{11} & X_{12} & \cdots & X_{1n} \\ X_{21} & X_{22} & \cdots & X_{2n} \\ \vdots & \vdots & \ddots & \vdots \\ X_{n1} & X_{n2} & \cdots & X_{nn} \end{bmatrix}.$$
(13)

They furthermore prove that there is no duality gap between the primal problem (11) and its dual problem (12) if the maximum residuals stay below a certain threshold. If R^* is the global optimum of problem (11), the solution of problem (12) satisfies

$$X^{\star} = R^{\star T} R^{\star}. \tag{14}$$

For readers who are interested in the duality gap and global optimality proof, we kindly refer them to [18] for more details.

Problem (12) is an SDP problem [6]. Since every $X \succeq 0$ can be factored as Y^TY for some Y [7], and—in the case of rotation averaging—the optimal value of X satisfies $X^* = R^*TR^*$ [18], there is an implicit constraint on X such that $\operatorname{rank}(X) = 3$. Thus, X can be reformulated as

$$X = Y^T Y, (15)$$

where $Y = [Y_1 \ Y_2 \ \cdots \ Y_n], Y_i^T Y_i = I, \forall i \in [n]$. By substituting (15) into problem (12), a new problem is obtained

$$\min_{Y} - \operatorname{tr}(GY^{T}Y)$$
s.t. $Y = [Y_1 \ Y_2 \cdots Y_n], \quad Y_i^{T}Y_i = I, \forall i \in [n].$ (16)

Tian *et al* [37] proposed a block coordinate minimisation (BCM) method to solve the low-rank SDP problem (16). The update of Y_j in problem (16) is determined by [37]

$$Y_j^{\star} = U_j I_{3 \times 3} V_j^T = U_j V_j^T, \tag{17}$$

where $U_j \Sigma V_j$ is the singular value decomposition of $-Q_j$.

In Algorithm 1, we outline the BCM with graph sparsity. In steps $6\sim7$ of Algorithm 1, the time complexity of O(n) is only an upper bound occurring for general cases. In practice, due to the commonly sparse structure of SfM problems, time complexity can be further reduced to O(d), where d is the degree of the nodes. This property is important for accelerating the optimisation. Notice that, with our fast view graph filtering, the graph can be more sparse and we can gain more acceleration.

Algorithm 1 BCM for SDP [37] with Graph Sparsity

```
Input: relative rotations \mathcal{R}_{\mathrm{rel}}, maxIterNum, Y^0.

Output: First-order critical point Y^*

1: k \leftarrow 0; Q_j^0 \leftarrow \sum_{i \neq j}^n Y_i G_{ij}, \forall j \in [n].

2: while k < maxIterNum & not converge do

3: for i < n do

4: j_k \leftarrow i

5: Update Y_{j_k}^{k+1} by Eq. (17)

6: for \forall j \neq j_k, G_{j_k j} \neq 0 do

7: Q_j^{k+1} \leftarrow Q_j^k + (Y_{j_k}^{k+1} - Y_{j_k}^k)G_{j_k j}

8: k \leftarrow k+1;

9: return Y
```

Discussion of Global Optimality: Problem (16) is nonconvex, and there is no guarantee that we can obtain the global optimum. In Wang's method [42], the global optimum is guaranteed by selecting an appropriate step size and random initialisation (Theorem 3.4). However, the theorem is only hold for variables that are scalar. For RA problem, global optimality is not hold since we optimised on manifold. Boumal [4] proposes a general framework

named the *Riemannian Staircase* algorithm (RS), which can find the global optimum. As previous work has applied a Riemannian based method to ensure the global optimum [33, 38, 17], we recommend interested readers to refer to them.

4.3. Local Refinement

The global optimisation presented in Sec. 4.2 assumes that the input relative rotations do not contain any outliers. As a result, it is sensitive to outliers. To further improve the robustness and accuracy of the low-rank BCM method, we follow the *suggest-and-improve* framework of [32]. The global optimisation approaches can obtain a good solution close to the global optimum. Still, it could be further refined by a gradient descent algorithm. We adopt this framework and use the method of Chatterjee and Govindu [9] as a local optimiser. This method performs an Iteratively Reweighted Least Square (IRLS) under Lie algebra, which leads to an efficient and robust optimiser. The rotation R_{ij}, R_i, R_j can be represented by the corresponding Lie algebra $\omega_{ij}, \omega_i, \omega_j$, respectively. Using the Baker-Campbell-Hausdorff (BCH) equation, the relationship of Eq. (5) can be converted to

$$\omega_{ij} = \omega_j - \omega_i. \tag{18}$$

By collecting the relative constraints, we obtain

$$A\boldsymbol{\omega}_{\text{global}} = \boldsymbol{\omega}_{\text{rel}}.$$
 (19)

Here A is a sparse matrix, in which all consecutive 3×3 blocks are zeros except two matrices I and -I. Encapsulating Eq. (19) with a Huber loss $\rho(x)=\frac{x^2}{x^2+\sigma^2}$, we can optimise a robust cost function under least square meaning

$$\underset{\boldsymbol{w}_{\text{global}}}{\arg\min} \sum \rho(\|A\boldsymbol{\omega}_{\text{global}} - \boldsymbol{\omega}_{\text{rel}}\|). \tag{20}$$

4.4. Hybrid of Global Rotation Averaging and Local Refinement

We outline our hybrid rotation averaging algorithm in Algorithm 2. An ablation study of robustness against outliers is shown in Fig. 2. The outlier ratio ranges from 0 to 50% and is incremented in steps of 5%. We display the mean rotation error over 30 experiments. As can be observed, both VGF and local refinement improve the robustness of the global rotation averaging approach.

5. Application to Structure-from-Motion

In this section, we apply our rotation averaging method to an incremental SfM pipeline, which is known to suffer from the drift problem. Our hybrid SfM pipeline can be summarised as follows: We first construct the view-graph and obtain global rotations from our proposed fast and robust rotation averaging approach. Next, we create a seed

Algorithm 2 Hybrid Rotation Averaging Algorithm

Input: relative rotations \mathcal{R}_{rel}

Output: global rotations $\mathcal{R} = \{R_1, R_2, \cdots, R_n\}$

- 1: Perform fast VGF as described in Sec. 4.1.
- 2: Calculate global rotations using Algorithm 1 (or any other global rotation averaging method).
- 3: Refine global rotations by solving problem (20).

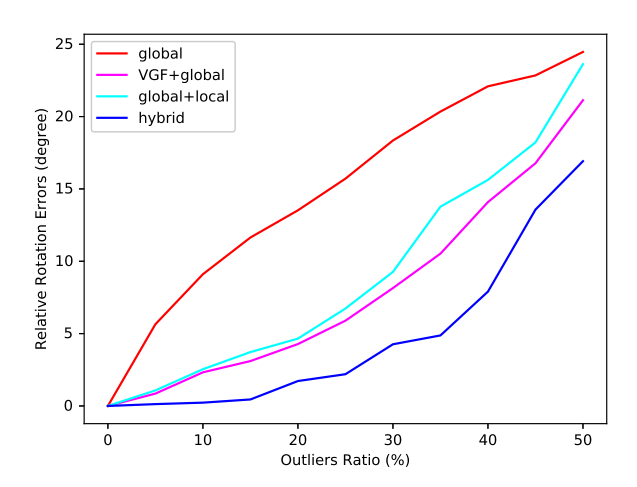


Figure 2. Ablation study of robustness. Outliers are generated by perturbing ground truth by rotation between $60^{\circ} - 90^{\circ}$. *global* represents the proposed low-rank BCM method, and *hybrid* represents the proposed hybrid method with VGF and local refinement.

reconstruction by selecting two appropriate images. We then continue by incrementally registering adjacent camera poses using a RANSAC-based [20] P3P [27] algorithm, and triangulate landmarks. To reduce the accumulation of errors in our incremental SfM pipeline, we perform local bundle adjustment after each successful registration of an image, and global bundle adjustment whenever the number of recently added views surpasses a certain threshold.

The drift problem is not solved, as each newly computed camera pose is affected by a small error, and these errors accumulate along the graph. Traditional incremental SfM pipelines have no way to rectify these errors. To tackle this problem, we introduce a novel cost function with averaged rotations as regularisers for bundle adjustment. Let \mathcal{I}_i denote the measurements of image i. Each image observes 3D landmarks given by the set \mathcal{P}_i . Let $\mathbf{u}_{il} \in \mathcal{I}_i$ furthermore denote the image keypoint measurement of landmark l in frame i. Grouping image measurements with the precomputed known rotations, we have

$$\mathcal{Z} = \left\{ \mathcal{I}_i, \hat{\mathcal{R}}_i, \hat{\mathcal{R}}_j | (i, j) \in \mathcal{E} \right\}$$
 (21)

In SfM, camera poses are estimated as well as 3D points observed by cameras. We have the following unknowns:

$$\mathcal{X}_i = \{R_i, C_i, \mathcal{P}_i\}, \ \mathcal{X} = \{\mathcal{X}_i | i \in [0, N]\},$$
 (22)

where R_i and C_i are the estimated camera rotation and center, respectively. Note that the sets \mathcal{P}_i are intersection, which—in a slight abuse of notation—is ignored for the sake of simplicity.

We first give the proposed cost function as below:

$$\sum_{i \in N} \sum_{l \in \mathcal{I}_i} \rho_v \left(\left\| \mathbf{r}_{\mathcal{I}_{il}} \right\|^2 \right) + \sum_{(i,j) \in \mathcal{E}} w_{ij} \left\| \mathbf{r}_{\mathcal{R}_{ij}} \right\|^2, \qquad (23)$$

where $\rho_v(\cdot)$ is a robust loss function, and w_{ij} is an individual weighting function for each known rotation term. In this paper, we fix w_{ij} as a constant. This objective divides into two terms which are explained as follows.

Visual Term: We adopt traditional re-projection error in bundle adjustment as our visual term

$$\mathbf{r}_{\mathcal{I}_{il}} = \mathbf{u}_{il} - \mathbf{\Pi}(R_i, C_i, \mathcal{P}_i, l), \tag{24}$$

where $\Pi(\cdot)$ is the back-projection function that projects landmarks into the image plane. Note that the latter also depends on camera intrincs, which—for the sake of a simplified and general notation—are not specified.

Known Rotation Term: The added known rotation term is

$$\mathbf{r}_{\mathcal{R}_{ij}} = \log(\hat{\mathcal{R}}_i^T \hat{\mathcal{R}}_i R_i^T R_j), \tag{25}$$

where log is the logarithm map $SO(3) \to \mathfrak{so}(3)$. This known rotation term is used as a regulariser in the complete cost function.

We further make an explanation for our cost function: the first one corresponds to the reprojection error, the second one is used to penalize the large RPE that is caused by poses drift. Since the reprojection error might be small even when camera poses drift (Because triangulated 3D points are geometrically coherent with camera poses), however, the known rotation term can measure the discrepancy between the averaged rotations and incrementally recovered rotations in this situation. Thus the optimiser tries to minimize this discrepancy, and poses drift is alleviated.

6. Experimental Results

Our experiments aim at demonstrating the accuracy, efficiency, and robustness of the proposed methods. We implement Levenberg-Marquardt (LM) [30], row-by-row block coordinate descent (RBR-BCD) [18], and our hybrid rotation averaging in C++. Besides, the implementation of SE-Sync [33] and Shonan [16] are obtained from the given websites of their papers. For HSfM [13] and LUD [31], we use [10] as the rotation averaging solver, and the Ceres solver [2] for bundle adjustment. All approaches are tested on a laptop with a 2.7 GHZ CPU and 8GB RAM.

6.1. Evaluation of Hybrid Rotation Averaging on Synthetic Datasets

We designed 7 synthetic datasets to evaluate the performance of our rotation averaging approach, The view and

relative rotation numbers are shown in Table 1, and denoted by n and #edges respectively. The ground truth absolute rotations are initialised randomly. The relative rotations are constructed by a spanning tree expanded by random edges until the given number of relative poses is reached. All relative rotations are derived from ground truth, and perturbed by random angular rotations about randomly selected axes. The perturbation angles are normally distributed with 0 mean and a variance of either $\sigma=0.2\,$ rad or $\sigma=0.5\,$ rad. Initial absolute rotations are chosen randomly.

The evaluation results are shown in Table 1, where we compare our method against LM [30], RBR-BCD [18], Shonan [16] and SE-Sync [33]. In terms of efficiency, RBR-BCD is the slowest and almost 1000 times slower than others when n = 1000. SE-Sync is faster than LM but stays within the same order of magnitude. While SE-Sync is slightly faster than ours when cameras number is below 500, the hybrid rotation averaging approach is $1 \sim 2$ orders of magnitude faster than SE-Sync when the number of views grows beyond 1000. While Shonan is also a lowrank method, as well as SE-Sync and ours, it is almost 2 magnitude slower than SE-Sync, and 3 magnitude slower than ours. In terms of the scale of the solved problems, RBR-BCD failed when the camera number increased to 5000, 10000, or 50000. This is primarily due to insufficient memory for optimisation, and we marked the corresponding cells in the table by "-". LM, Shonan and SE-Sync failed when the camera number reaches 50000, as there is insufficient memory to hold the Jacobian matrix. Besides, Shonan is not converged when camera number is 10000 with variance 0.5, and we marked the corresponding cells by "NC". As BCM approach only needs to compute the SVD of a small block matrix and evaluate d matrix operations of 3×3 matrices in each iteration, we are able to solve all the evaluated large-scale datasets.

In terms of accuracy, LM achieves the global optimum with certain probability (30% - 70%) as reported in [18]), and Table 1 only shows the best results. While all the evaluated globally optimal methods have the same accuracy and can both obtain the global optimum for successful cases.

6.2. Evaluation of RA-SfM on Real-World Datasets

We evaluate the performance of our RA-SfM on large scale real-world datasets and compare it against state-of-the-art incremental [34], global [31] and hybrid [13] SfM approaches. Since the quasi-convex SfM approach [48] is sensitive to outlies and extremely slow in such datasets, we did not evaluate it in our experiment.

Figure 3 shows the reconstruction results of COLMAP and our RA-SfM on the Campus [15] dataset. This dataset, which has a loop, mainly contains plants that can produce lots of wrong matching results. COLMAP [34] fails to reconstruct this dataset, as the camera poses drift and the loop

	11		*******			~~~			~~~				
n	#edges	σ	LM [30]		RBR-BCD [18]		Shona	ı n [16]	SE-Syr	ıc [33]	hybrid RA		
11	πcuges	0	\bar{R}	time(s)	\bar{R}	time(s)	\bar{R}	time(s)	\bar{R}	time(s)	\bar{R}	time(s)	
20	20 30	0.2	1.800e-03	0.001	1.813e-06	0.007	1.719e-06	0.089	1.499e-06	< 1e-06	1.502e-06	< 1e-06	
20	30	0.5	1.799e-01	0.002	2.634e-02	0.013	2.633e-02	0.112	2.634e-02	< 1e-06	2.633e-02	0.001	
100	300	0.2	5.328e-03	0.007	2.607e-06	0.526	2.596e-06	0.787	2.589e-06	0.003	2.588e-06	0.003	
100	300	0.5	5.315e-01	0.014	3.788e-02	0.530	3.591e-02	0.870	3.788e-02	0.003	3.788e-02	0.011	
500	1000	0.2	1.483e-03	0.264	3.008e-06	176.316	2.995e-06	18.47	2.901e-06	0.079	2.994e-06	0.006	
500 100	1000	0.5	1.225e-01	0.330	4.369e-02	4.369e-02 186.311		26.60	4.369e-02 0.079		4.369e-02	0.051	
1000 4000	4000	0.2	1.800e-01	0.321	2.810e-06	2,362	2.731e-06	22.730	2.641e-06	0.372	2.490e-06	0.008	
	4000	0.5	2.210e-01	0.237	3.790e-02	2,579	3.988e-02	29.57	3.930e-02	0.343	4.100e-02	0.105	
5000	20000	0.2	1.800e-01	7.083	-	-	2.335e-06	159.638	2.190e-06	4.63	2.246e-06	0.052	
3000	20000	0.5	3.980e-01	7.375	-	-	3.977e-02	340.116	3.800e-02	3.95	3.800e-02	0.441	
10000	40000	0.2	1.320e-01	24.256	-	-	2.375e-06	1108.435	2.012e-06	13.398	2.012e-06	0.092	
10000	40000	0.5	2.340e-01	24.071	-	-	NC	NC	3.612e-02	15.205	3.600e-02	1.042	
50000	200000	0.2	-	-	-	-	-	-	-	-	2.941e-06	0.602	
30000 200000	200000	0.5	-	-	-	-	-	-	-	-	5.000e-02	6.193	

Table 1. Comparison of runtime on synthetic datasets. n is the number of rotations, \bar{R} represents the average rotation error (unit: degree).



Figure 3. Reconstruction results for the Campus dataset [15]. Left: COLMAP [34], Right: Our RA-SfM.

is not closed. Our approach closes the loop successfully, as the known rotation optimisation is able to further constrain camera poses after the initial registration.

We also evaluated our approach on the online datasets from [45], which are collections of challenging unordered images. The datasets contains many wrong epipolar geometries due to extreme viewpoint, scale and illumination changes. The runtime and accuracy results are shown in Table 2. As can be observed, our approach recovers the most camera poses in all online datasets, and has the lowest mean reprojection error (MRE) in most of the online datasets. For our RA-SfM, the time for rotation averaging is separately given. COLMAP [34] is the second best approach in terms of recovered camera poses and MRE, which shows the robustness of incremental SfM approaches. While LUD [31] is the most efficient among the evaluated approaches, it has large MRE, and the recovered camera poses is less than ours or even COLMAP. HSfM [13] is faster than COLMAP and our approach, because it only samples 2 correspondences to compute the camera center in each RANSAC iteration. HSfM [13] recovers the fewest camera poses, and fails to recover the correct camera centers.

Some visual results for online datasets are shown in Fig. 4. For each sub-figure, the top and bottom images are the results obtained by COLMAP [34] and our RA-SfM, respectively. For Ellis Island dataset, we showed two different parts in the first two columns of Fig. 4, where the red rectangle area shows the comparison result. For Gendarmen-

markt dataset, the reconstruction result of COLMAP is bad on the left part, which indicates wrong camera poses. For Vienna Cathedral dataset, our approach can recover more scene details than COLMAP, as is again indicated by the red rectangle.

7. Conclusion

This paper presents a hybrid rotation averaging method that is robust to outliers. We combine the existing global and local RA methods, with fast view graph filtering is applied at first to increase graph sparsity, so as to accelerate optimisation. The exposition is rounded off by a soft embedding into an incremental SfM pipeline leading to accurate, reliable, and highly efficient results.

References

- [1] Baker-campbell-hausdorff formula. https: //en.wikipedia.org/wiki/Baker-Campbell-Hausdorff_formula.
- [2] Sameer Agarwal and Keir Mierle. Ceres solver. http://ceres-solver.org.6
- [3] Sameer Agarwal, Noah Snavely, Ian Simon, Steven M. Seitz, and Richard Szeliski. Building rome in a day. In *IEEE 12th International Conference on Computer Vision*, pages 72–79, 2009.
- [4] Nicolas Boumal. A riemannian low-rank method for optimization over semidefinite matrices with block-diagonal constraints. *CoRR*, abs/1506.00575, 2015. 1, 2, 4
- [5] Stephen P. Boyd, Neal Parikh, Eric Chu, Borja Peleato, and Jonathan Eckstein. Distributed optimization and statistical learning via the alternating direction method of multipliers. Foundations and Trends in Machine Learning, 3(1):1–122, 2011. 2
- [6] Stephen P. Boyd and Lieven Vandenberghe. *Convex Optimization*. Cambridge University Press, 2014. 2, 4
- [7] Samuel Burer and Renato D. C. Monteiro. A nonlinear programming algorithm for solving semidefinite programs

Table 2. Comparison of runtime and accuracy on online datasets [45]. N_i denotes the number of images, N_c denotes the number of
registered cameras, N_p denotes the reconstructed 3D landmarks, MRE means mean reprojection error in pixel.

Dataset	N_i	COLMAP [34]			LUD [31]			HSfM [13]				RA-SfM						
Dataset		N_c	N_p	MRE (px)	T(s)	N_c	N_p	MRE (px)	T(s)	N_c	N_p	MRE (px)	T(s)	N_c	N_p	MRE (px)	$R_t(s)$	T(s)
Alamo	2,915	666	94K	0.68	882	578	146K	1.28	260	522	149K	1.62	1,079	895	141K	0.65	3.84	2,784
Ellis Island	2,587	315	64K	0.70	332	234	16K	1.54	24	208	34K	2.53	169	727	146K	0.72	6.4	3,954
Gendarmenmarkt	1,463	861	123K	0.68	627	705	87K	1.51	104	542	74K	1.94	377	1,023	202K	0.70	6.2	3,903
Madrid Metropolis	1,344	368	43K	0.60	251	350	51K	1.08	36	292	51K	1.48	221	438	66K	0.59	2.2	1,440
Montreal N.D.	2,298	506	98K	0.81	723	462	166K	1.64	194	418	155K	1.95	1041	528	105K	0.67	1.7	1,446
Notre Dame	1,431	1408	349K	0.76	22,788	550	262K	2.06	259	526	281K	2.30	2,375	1,409	353K	0.75	1.7	3,323
NYC Library	2,550	453	77K	0.69	420	336	70K	1.52	75	282	74K	1.99	356	519	100K	0.65	2.1	1,734
Piazza del Popolo	2,251	437	47K	0.72	380	329	38K	1.65	62	286	35K	1.92	212	966	122K	0.66	4.3	3,228
Piccadilly	7,351	2,336	260K	0.75	1,961	2,301	202K	1.83	262	1,665	185K	2.09	2,169	3,041	363K	0.80	23.8	15,324
Roman Forum	2,364	1,409	222K	0.70	1,041	1,045	256K	1.71	182	1,071	262K	1.93	2,237	1,460	267K	0.77	4.6	5,502
Tower of London	1,576	578	109K	0.61	678	485	140K	1.65	95	398	149K	1.91	816	672	139K	0.58	2.2	2,040
Trafalgar	15,685	5,211	450K	0.74	5,122	5,044	378K	1.56	713	3,446	318K	1.95	5,761	7,085	597K	0.72	58.5	15,048
Union Square	5,961	763	53K	0.67	693	803	41K	1.65	107	769	38K	1.88	1,763	809	57K	0.52	4.5	1,962
Vienna Cathedral	6,288	933	190K	0.74	1,244	849	203K	1.91	173	662	252K	2.36	2,307	1,173	303K	0.71	9.4	1,611
Yorkminster	3,368	456	105K	0.70	997	421	132K	1.75	135	417	129K	1.93	1,487	614	183K	0.64	5.8	926



Figure 4. Visual reconstruction results for some of the online datasets [45]. For each sub-figure, the top and bottom images are respectively the results obtained from COLMAP [34] and our RA-SfM. (The first two columns are results of two parts of the Ellis Island datasets.)

via low-rank factorization. *Math. Program.*, 95(2):329–357, 2003. 2, 4

- [8] Álvaro Parra Bustos, Tat-Jun Chin, Anders P. Eriksson, and Ian D. Reid. Visual SLAM: why bundle adjust? In *International Conference on Robotics and Automation*, 2019.
- [9] Avishek Chatterjee and Venu Madhav Govindu. Efficient and robust large-scale rotation averaging. In *IEEE International Conference on Computer Vision*, pages 521–528, 2013. 1, 2, 3, 5
- [10] Avishek Chatterjee and Venu Madhav Govindu. Robust relative rotation averaging. *IEEE Trans. Pattern Anal. Mach. Intell.*, 40(4):958–972, 2018. 2, 3, 6
- [11] David J. Crandall, Andrew Owens, Noah Snavely, and Dan Huttenlocher. Discrete-continuous optimization for largescale structure from motion. In *IEEE Conference on Com-*

- puter Vision and Pattern Recognition, pages 3001–3008, 2011. 2
- [12] David J. Crandall, Andrew Owens, Noah Snavely, and Daniel P. Huttenlocher. SfM with MRFs: Discretecontinuous optimization for large-scale structure from motion. *IEEE Trans. Pattern Anal. Mach. Intell.*, 35(12):2841– 2853, 2013. 2
- [13] Hainan Cui, Xiang Gao, Shuhan Shen, and Zhanyi Hu. Hsfm: Hybrid structure-from-motion. In *IEEE Conference* on Computer Vision and Pattern Recognition, pages 2393– 2402, 2017. 2, 6, 7, 8
- [14] Hainan Cui, Shuhan Shen, Xiang Gao, and Zhanyi Hu. Batched incremental structure-from-motion. In *International Conference on 3D Vision*, pages 205–214, 2017. 2
- [15] Zhaopeng Cui and Ping Tan. Global structure-from-motion by similarity averaging. In *IEEE International Conference*

- on Computer Vision, pages 864–872, 2015. 1, 2, 6, 7
- [16] Frank Dellaert, David M. Rosen, Jing Wu, Robert Mahony, and Luca Carlone. Shonan rotation averaging: Global optimality by surfing $SO(p)^n$. In European Conference on Computer Vision, volume 12351, pages 292–308. Springer, 2020. 1, 2, 6, 7
- [17] Frank Dellaert, David M. Rosen, Jing Wu, Robert Mahony, and Luca Carlone. Shonan rotation averaging: Global optimality by surfing so(p)ⁿ. CoRR, abs/2008.02737, 2020. 2,
- [18] Anders Eriksson, Carl Olsson, Fredrik Kahl, and Tat-Jun Chin. Rotation averaging with the chordal distance: Global minimizers and strong duality. *IEEE Trans. Pattern Anal. Mach. Intell.*, 2020. 1, 2, 3, 4, 6, 7
- [19] Anders P. Eriksson, Carl Olsson, Fredrik Kahl, and Tat-Jun Chin. Rotation averaging and strong duality. In *IEEE Con*ference on Computer Vision and Pattern Recognition, pages 127–135, 2018.
- [20] Martin A. Fischler and Robert C. Bolles. Random sample consensus: A paradigm for model fitting with applications to image analysis and automated cartography. *Commun. ACM*, 24(6):381–395, 1981. 5
- [21] Johan Fredriksson and Carl Olsson. Simultaneous multiple rotation averaging using Lagrangian duality. In *Asian Conference on Computer Vision*, volume 7726, pages 245–258, 2012. 2
- [22] Thomas Goldstein, Paul Hand, Choongbum Lee, Vladislav Voroninski, and Stefano Soatto. Shapefit and shapekick for robust, scalable structure from motion. In *Computer Vision* - ECCV 2016 - 14th European Conference, pages 289–304, 2016. 1
- [23] Venu Madhav Govindu. Combining two-view constraints for motion estimation. In *IEEE Computer Society Conference on Computer Vision and Pattern Recognition*, pages 218–225, 2001. 1, 2, 3
- [24] Venu Madhav Govindu. Lie-algebraic averaging for globally consistent motion estimation. In *IEEE Computer Society Conference on Computer Vision and Pattern Recognition*, pages 684–691, 2004. 2, 3
- [25] Richard I. Hartley, Jochen Trumpf, Yuchao Dai, and Hong-dong Li. Rotation averaging. *International Journal of Computer Vision*, 103(3):267–305, 2013. 3
- [26] Nianjuan Jiang, Zhaopeng Cui, and Ping Tan. A global linear method for camera pose registration. In *IEEE International Conference on Computer Vision*, pages 481–488, 2013.
- [27] Laurent Kneip, Davide Scaramuzza, and Roland Siegwart. A novel parametrization of the perspective-three-point problem for a direct computation of absolute camera position and orientation. In *The 24th IEEE Conference on Computer Vision* and Pattern Recognition, pages 2969–2976, 2011. 5
- [28] Yi Ma, Stefano Soatto, Jana Košecká, and S. Shankar Sastry. *An Invitation to 3-D Vision: From Images to Geometric Models*. Springer Science & Business Media, 2012. 3
- [29] Pierre Moulon, Pascal Monasse, and Renaud Marlet. Global fusion of relative motions for robust, accurate and scalable structure from motion. In *IEEE International Conference on Computer Vision*, pages 3248–3255, 2013. 1, 2

- [30] Jorge Nocedal and Stephen J. Wright. *Numerical Optimization*. Springer, 1999. 6, 7
- [31] Onur Özyesil and Amit Singer. Robust camera location estimation by convex programming. In *IEEE Conference* on Computer Vision and Pattern Recognition, pages 2674– 2683, 2015. 1, 6, 7, 8
- [32] Jaehyun Park and Stephen Boyd. General heuristics for nonconvex quadratically constrained quadratic programming. arXiv:1703.07870, 2017. 5
- [33] David M Rosen, Luca Carlone, Afonso S Bandeira, and John J Leonard. SE-Sync: A certifiably correct algorithm for synchronization over the special Euclidean group. *International Journal of Robotics Research*, 38(2-3):95–125, 2019. 1, 2, 5, 6, 7
- [34] Johannes L. Schönberger and Jan-Michael Frahm. Structurefrom-motion revisited. In 2016 IEEE Conference on Computer Vision and Pattern Recognition, pages 4104–4113, 2016. 2, 6, 7, 8
- [35] Tianwei Shen, Siyu Zhu, Tian Fang, Runze Zhang, and Long Quan. Graph-based consistent matching for structure-frommotion. In *European Conference on Computer Vision*, volume 9907, pages 139–155, 2016. 3
- [36] Chris Sweeney, Torsten Sattler, Tobias Höllerer, Matthew Turk, and Marc Pollefeys. Optimizing the viewing graph for structure-from-motion. In *IEEE International Conference on Computer Vision*, pages 801–809, 2015. 1, 2
- [37] Yulun Tian, Kasra Khosoussi, and Jonathan P. How. Block-coordinate minimization for large SDPs with block-diagonal constraints. arXiv: 1903.00597, 2019. 2, 3, 4
- [38] Yulun Tian, Kasra Khosoussi, David M. Rosen, and Jonathan P. How. Distributed certifiably correct pose-graph optimization. arXiv: 1911.03721, 2019. 2, 5
- [39] Bill Triggs, Philip F. McLauchlan, Richard I. Hartley, and Andrew W. Fitzgibbon. Bundle adjustment - A modern synthesis. In Vision Algorithms: Theory and Practice, International Workshop on Vision Algorithms, pages 298–372, 1999.
- [40] Roberto Tron, Xiaowei Zhou, and Kostas Daniilidis. A survey on rotation optimization in structure from motion. In IEEE Conference on Computer Vision and Pattern Recognition Workshops, pages 1032–1040, 2016.
- [41] Lanhui Wang and Amit Singer. Exact and stable recovery of rotations for robust synchronization. *Information and Infer*ence, 2(2):145–194, 2013. 2
- [42] Po-Wei Wang, Wei-Cheng Chang, and J. Zico Kolter. The mixing method: coordinate descent for low-rank semidefinite programming. arXiv: 1706.00476, 2017. 2, 4
- [43] Zaiwen Wen, Donald Goldfarb, Shiqian Ma, and Katya Scheinberg. Row by row methods for semidefinite programming. Technical report, 2009. 2
- [44] Zaiwen Wen, Donald Goldfarb, and Wotao Yin. Alternating direction augmented lagrangian methods for semidefinite programming. *Math. Program. Comput.*, 2(3-4):203–230, 2010.
- [45] Kyle Wilson and Noah Snavely. Robust global translations with 1dsfm. In *Computer Vision European Conference*, pages 61–75, 2014. 1, 7, 8

- [46] Changchang Wu. Towards linear-time incremental structure from motion. In 2013 International Conference on 3D Vision, pages 127–134, 2013. 2
- [47] Christopher Zach, Manfred Klopschitz, and Marc Pollefeys. Disambiguating visual relations using loop constraints. In IEEE Conference on Computer Vision and Pattern Recognition, pages 1426–1433, 2010. 3
- [48] Qianggong Zhang, Tat-Jun Chin, and Huu Minh Le. A fast resection-intersection method for the known rotation problem. In 2018 IEEE Conference on Computer Vision and Pattern Recognition, pages 3012–3021, 2018. 6
- [49] Siyu Zhu, Tianwei Shen, Lei Zhou, Runze Zhang, Jinglu Wang, Tian Fang, and Long Quan. Parallel structure from motion from local increment to global averaging. *arXiv:* 1702.08601, 2017. 1, 2
- [50] Siyu Zhu, Runze Zhang, Lei Zhou, Tianwei Shen, Tian Fang, Ping Tan, and Long Quan. Very large-scale global SfM by distributed motion averaging. In *IEEE Conference* on Computer Vision and Pattern Recognition, pages 4568– 4577, 2018. 1, 2
- [51] Bingbing Zhuang, Loong-Fah Cheong, and Gim Hee Lee. Baseline desensitizing in translation averaging. In *IEEE Conference on Computer Vision and Pattern Recognition*, pages 4539–4547, 2018. 1